Electronic Supplementary Material (ESI) for Physical Chemistry Chemical Physics.

SI: Designing new SRP density functionals including non-local vdW-DF2 correlation for H_2 + Cu(111) and their transferability to H_2 + Ag(111), Au(111) and Pt(111)

Egidius W.F. Smeets and Geert-Jan Kroes*

Leiden Institute of Chemistry, Gorlaeus Laboratories, Leiden University, P.O. Box 9502, 2300 RA, The Netherlands

E-mail: g.j.kroes@chem.leidenuniv.nl

Supporting text

S1 CRP interpolation of PESs

In principle we use the following grids: $r \in \{0.4, 0.5, 0.6, 0.65, 0.7, 0.75, 0.8, 0.85, 1.0, 1.25, 1.5, 1.75, 2.0, 2.3\}$ Å and $Z \in \{0.25, 0.5, 0.75, 1.0, 1.25, 1.5, 1.75.2.0, 2.25, 2.5, 2.75, 3.0, 3.25, 3.5, 3.75, 4.0, 4.25, 4.5, 4.75, 5.0, 5.5, 6.0, 7.0\}$ Å for the 29 two dimensional cuts of the six dimensional molecular PES are used. For the atomic PES a grid denoted by $Z \in [-1.2 : 9]$ Å with $dZ = 0.075$ Å for $Z \leq 2$ Å and $dZ = 0.15$ Å for $Z > 2$ Å for all but the reference site was used. For the atomic reference site a dZ of 0.025 Å was used for $Z < 2$ Å. Note that in the case of the atomic PES hard to converge geometries can be discarded and additional points can be added at random Z to improve the quality of the resulting CRP PES.

S2 Quantum Dynamics

We construct the initial wave function as a product of a rovibrational eigenfunction of H_2 in the gas phase characterized by the initial vibrational quantum number ν, the initial angular momentum quantum number J and the initial magnetic rotational quantum number m_J, i.e. $\Phi_{\nu,J,m_J}(r, \theta, \phi)$, and a Gaussian wave packet describing translational motion with the initial wave vector $\vec{k}_0 = (k_0^X, k_0^Y, k_0^Z)^{\mathrm{T}}$

$$\Psi(\vec{Q}, t = 0) = \Phi_{\nu,J,m_J}(r, \theta, \phi)\psi(\vec{k}_0, t_0) \tag{S1}$$

The initial translational motion is then described by the following wave function:

$$\psi(\vec{k}_0, t_0) = e^{i(k_0^X X_0 + k_0^Y Y_0)} \int_{-\infty}^{\infty} \beta(k_0^Z) e^{ik_0^Z Z_0} dk_0^Z \tag{S2}$$

Here, $\beta(k_0^Z)$ is the initial Gaussian wave packet centered around Z_0, which is defined through the width parameter σ and average momentum $\overline{k}$ according to:

$$\beta(k_0^Z) = \left(\frac{2\sigma^2}{\pi}\right)^{-\frac{1}{4}} e^{-\sigma^2(\overline{k}-k_0^Z)} e^{-i(\overline{k}-K_0^Z)Z_0}. \tag{S3}$$

The initial momentum of the wave packet is derived from the minimum and maximum translational energy in the Z direction of the wave packet (see E_{min} and E_{max} in table S1), as we did not perform QD calculations with initial transverse momentum k_0^X and k_0^Y are taken to be zero for all calculations. The initial wave function is propagated using the split operator approach with time step Δt.[1] At large Z and r we employ quadratic complex absorbing potentials,[2] which allows us to use short grids by avoiding reflection of the wave packet at grid boundaries. The scattered wave packet is analysed using the scattering matrix formalism,[3] and subsequently the sticking probability is computed by subtracting the sum of the scattering probabilities from one.

All parameters describing the grids, optical potentials, time step, the initial wave packet, the rovibrational basis set, and all the rovibrational states for which calculations have been carried out, are tabulated in table S1. Note that all rovibrational states that have a Boltzmann weight > 0.001, at the nozzle temperature of 2000K, are included.

S3 Methods for determining parameters describing initial-state selected reaction probabilities from associative desorption experiments

S3.1 Method A1

In method A1, it is assumed that the effective barrier heights ($E_0(\nu, J)$) can be kept the same in the description of the sticking and the associative desorption experiments, even though these are done at quite different temperatures.[4,5] The surface temperature dependence of

$P_{\mathrm{deg}}(E,\nu,J)$ is taken into account by choosing the $W_{\nu,J}$ parameters larger in the description of the associative desorption experiments (done at high T_s, typically $>$ 900 K) than in the sticking experiments (done at low T_s, usually lower than room temperature), on the basis of experiments.[6,7] Next, the $A_{\nu,J}$ parameters are determined assuming that they do not depend on T_s, by requiring that the measured sticking probabilities can be computed according to Eqs. 4-9. In this procedure, the A parameters are typically taken either independent of the initial rovibrational state, or dependent only on ν to obtain a fitting procedure with a properly constrained number of degrees of freedom. In the latter case, one might use information regarding the relative values of the $A_{\nu,J}$ parameters extracted from the experiments. Procedure A1 was followed to extract initial-state resolved reaction probabilities in experiments on H_2 and D_2 desorbing from Cu(111).[4,5,8]

A comparison between theory and experiment can then be made in terms of $E_{1/2}(\nu,J)$ parameter values extracted from theory, which represent the incidence energy at which the computed reaction probability becomes equal to half the experimental saturation value $A_{\nu,J}$,[9] and the experimental values of $E_0(\nu,J)$. Procedure A1 is illustrated in figure S1a for H_2 + Cu(111) and in figure S1c for D_2 + Cu(111). A disadvantage of procedure A1 is that assuming that $E_{1/2}(\nu,J)$ parameters can be compared with $E_0(\nu,J)$ parameters presumes, in a way, that the saturation value of the computed sticking probability curve is the same as that of the measured one, which needs not be the case. This is one of the reasons that, in comparisons between theory and experiment, the procedure followed usually does not involve simply fitting computed reaction probabilities to Eq. 11 and then comparing the computed parameters of Eq. 11 directly to the experimental values. Using Eq. 11 to fit experimental reaction probabilities is at best a procedure to represent these probabilities over the range of energies from which they can be extracted with reasonable accuracy using Eq. 10. The error function fit form is not the most accurate expression to fit reaction probability curves for D_2 + Cu(111),[10] and comparison to theory suggests that using this expression does not yield an accurate extrapolation procedure to energies that exceed the energy range that can be used

for the experimental extraction procedure (Eq. 10). We also note that the characteristic energies $E_{1/2}(\nu, J)$ will not usually be inflexion points of the theoretical reaction probability curves.

S3.2 Method B1

In method B1, the experimental sticking probability curve is normalized by equating the reaction probability at $E_{\max}(\nu, J)$ to the computed value:[8,11]

$$A^{\mathrm{B1}}_{\nu,J} = P^{\mathrm{exp}}_{\mathrm{deg}}(E_{\max}(\nu, J)) \equiv P^{\mathrm{exp}}_{\mathrm{th}}(E_{\max}(\nu, J)) \tag{S4}$$

In procedure B1, the thus extracted reaction probability is simply set equal to $A_{\nu,J}$. Theory is then compared with experiment by extracting the theoretical characteristic energy $E_{1/2}(\nu, J)$ using:

$$P^{\mathrm{exp}}_{\mathrm{th}}(E_{1/2}(\nu, J)) = \frac{1}{2} A^{\mathrm{B1}}_{\nu,J} \tag{S5}$$

Method B1 is illustrated in figure S1b for H_2 + Cu(111), and in figure S1d for D_2 + Cu(111). Even though $E_{\max}(\nu, J)$ will usually not be big enough for $P_{\mathrm{deg}}(E_{\max}(\nu, J), \nu, J)$ to essentially equal the absolute A at high translational energy, the approximate $E_{1/2}(\nu, J)$ extracted in this way will be rather accurate as long as $P_{\mathrm{deg}}(E_{\max}(\nu, J), \nu, J) \geq 0.9\mathrm{A}$, in which case $E_{1/2}(\nu, J)$ will be underestimated by no more than $0.09\ W_{\nu,J}$, with $W_{\nu,J}$ typically being 0.2 eV for H_2 + Cu(111)[8] and 0.3 eV for H_2 + Au(111).[11] This condition is met if $E_{\max}(\nu, J) > E_0(\nu, J) + 0.9\ W_{\nu,J}$. Figure S2 shows that this is not the case for H_2 (D_2) + Au(111).

S3.3 Method B2

As already mentioned for H_2 + Au(111), we found that $E_{\max}(\nu, J)$ was typically not large enough to extract $E_{1/2}(\nu, J)$ parameters accurately using method B1. For H_2 + Au(111) we therefore use what we call method B2, which, to our knowledge, has not been used before. In this case we determine $P^{\mathrm{exp}}_{\mathrm{deg}}(E_{\max}(\nu, J))$ from theory, but we then also use the

measured $E_0(\nu, J)$ and $W_{\nu,J}$ value to determine the $A_{\nu,J}$ value at which the experimental reaction probability curve extracted in this way should saturate according to the fit (Eq. 11). Then the characteristic theoretical $E_{1/2}(\nu, J)$ value is obtained by requiring that $P_{\mathrm{deg}}(E_{1/2}(\nu, J), \nu, J) = 0.5 A^{\mathrm{B2}}_{\nu,J}$. This effectively means that we take the $A_{\nu,J}$ resulting from method B1 ($A^{\mathrm{B1}}_{\nu,J}$) and scale it accordingly:

$$A^{\mathrm{B2}}_{\nu,J} = \frac{A^{\mathrm{B1}}_{\nu,J}}{0.5 + 0.5 erf\left(\frac{E_{\max}(\nu,J) - E_0(\nu,J)}{W_{\nu,J}}\right)} \tag{S6}$$

Saturation values extracted using method B1 and B2 are compared to the experimental saturation values[11] for H_2 + Au(111) in figure S3a and for D_2 + Au(111) in figure S3b. Here, we should remember that the experimental saturation values are not on an absolute scale (they were determined using method A2). As will be shown in figure S3, the $A(\nu, J)$ parameters determined using method B1 and B2 do not vary much with ν and J, as expected from theory. Also, as expected, they tend not to exceed unity.

S4 The rotational hindering effect as obtained with the Dai-Zhang LEPS PES

We are aware of one single PES that does reproduce the rotational hindering effect as observed in the experiment, namely the LEPS PES[12] used by Dai and Light[13] for six-dimensional QD calculations. Dai and Light[13] reported a rotational hindering effect that is much stronger than we observe in all our data sets. We suspected that strong rotational hindering might be due to the use of an unconverged basis set or a too large time step used in the original QD calculations[13] or an inaccurate LEPS PES fit, or a combination of the two. We have recalculated the results reported by Dai and Light[13] which they present in their figure 1a[13] using the same LEPS potential[12] but with the QD input parameters of table S1 that are known to yield converged results. Our results are shown in figure S4b. Our converged TDWP calculations yield reaction probabilities that are somewhat lower than those

reported by Dai and Light[13], but our results for the ground state do however agree very well with those published by Somers et al.[14] who used the same potential.

$E_{1/2}(\nu, J)$ parameters calculated using method A1 and B1 and using the QD method for the B86SRP68-DF2 functional and the LEPS PES used by Dai and Light[13] are shown in comparison to experimental results for ($\nu = 0$) in figure S4c. The calculated $E_{1/2}(\nu, J)$ parameters for the B86SRP68-DF2 functional and the LEPS PES are in remarkably good agreement for $J \geq 3$ for both method A1 and B1. It is clear that the B86SRP68-DF2 functional somewhat underestimates the subtle rotational hindering effect when using procedure B1. Our converged QD calculations reproduce the original finding[13] that using the LEPS PES yields the rotational hindering trend. However, the results obtained for the LEPS PES used by Dai and Light[13] overestimate the observed rotational hindering effect when using either procedure A1 or B1. This leaves the accuracy of the PES as a possible culprit of the discrepancies observed between the results of our PESs and the results for the LEPS PES. We are unable to check the fit accuracy of the LEPS PES compared to the underlying electronic structure calculations,[15] which however are known to be unconverged.[12,15] We have however checked the fit accuracy of our CRP[16] PES for the B86SRP68-DF2 functional and found that our CRP[16] PES is highly accurate with respect to the underlying electronic structure calculations.

Since we do not observe the strong rotational hindering reported by Dai and Light[13] in any of the calculations we attempted for the reaction of H_2 with Cu(111) with our DFs, we believe that the large rotational hindering effect yielded by this particular LEPS PES must originate from inaccuracies still present in the LEPS fit or the underlying electronic structure calculations being unconverged. The good agreement between the results obtained using the LEPS PES[12] and our best SRP-DF for this system for $J \geq 3$ suggests that the observed rotational hindering is a very subtle effect.

Supporting figures

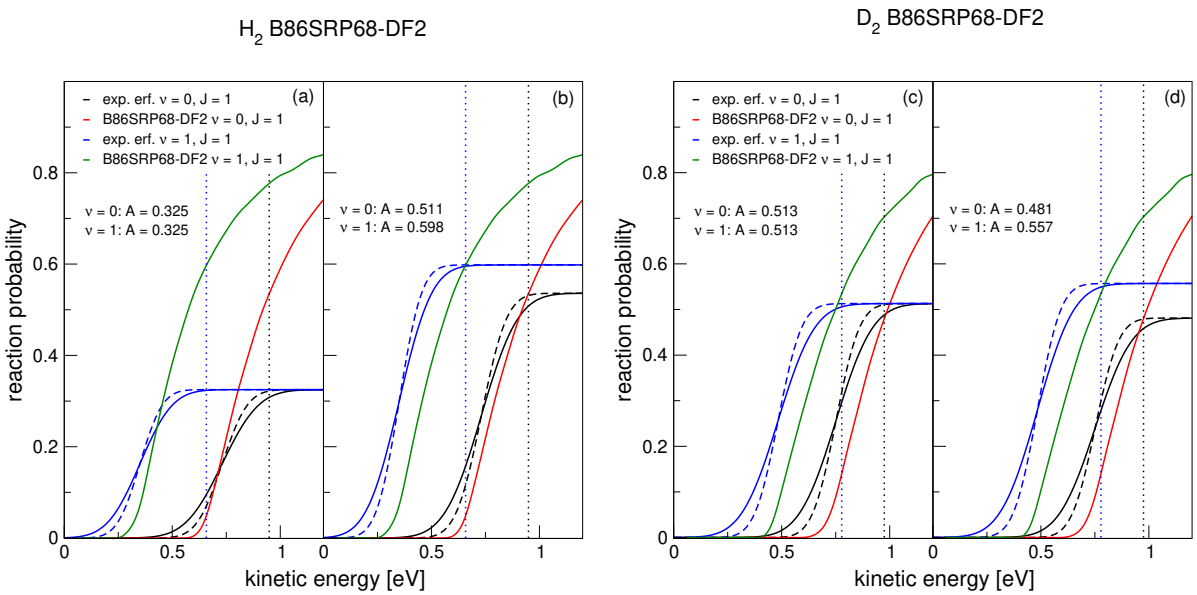

Figure S1: Reaction probability curves as a function of kinetic energy for H_2 + Cu(111) (a,b) and D_2 + Cu(111) (c,d). Experimental results[8] and QCT results obtained using the B86SRP68-DF2 SRP-DF are shown. Results for the ($\nu = 0, J = 1$) rovibrational state are shown with experimental results in black and theoretical results in red, and for the ($\nu = 1, J = 1$) rovibrational state are shown with experimental results in blue and theoretical results in green. Vertical dashed lines in the same color as the experimental results show $E_{\max}(\nu, J)$ for the corresponding state. Panels a and c illustrate method A1 to obtain $E_{1/2}(\nu, J)$ parameters and panels b and d method B1. The solid experimental lines use the measured $W(\nu, J)$ parameters[8] while the dashed experimental lines use the scaled $W(\nu, J)$ parameters as detailed in the supporting information of Ref.[8]

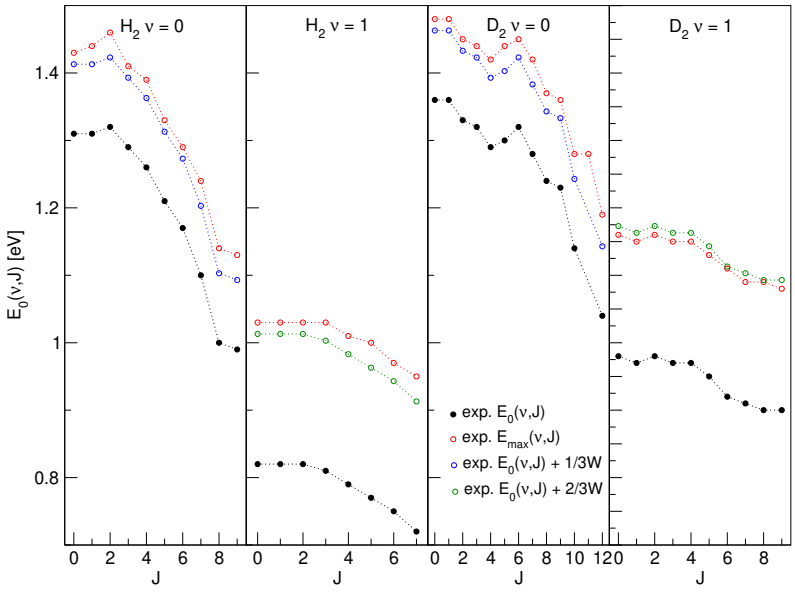

Figure S2: Measured[11] $E_0(\nu, J)$ parameters (black) and $E_{\max}(\nu, J)$ parameters (red) for H_2 (D_2) + Au(111) as a function of J. $E_0(\nu, J)$ parameters + $\frac{1}{3}$ W for ($\nu = 0$) (blue) and $E_0(\nu, J)$ parameters + $\frac{2}{3}$ W for ($\nu = 1$) (green) are shown as well.

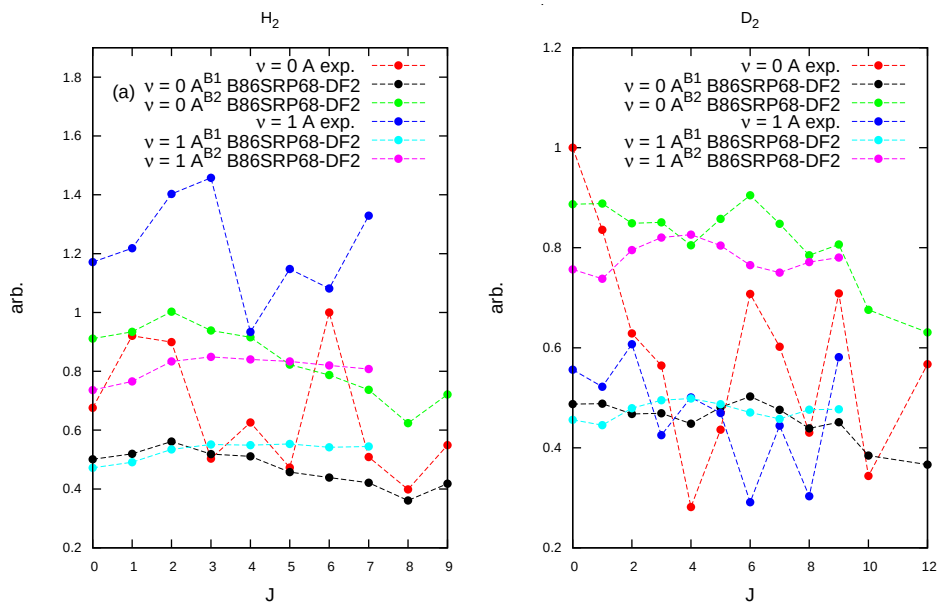

Figure S3: Comparison between the tabulated experimental[11] $A(\nu, J)$ values, red for ($\nu = 0$) and blue for ($\nu = 1$), the calculated $A^{\mathrm{B1}}(\nu, J)$ values computed using the B86SRP68-DF2 functional, black for ($\nu = 0$) and cyan for ($\nu = 1$), and the calculated $A^{\mathrm{B2}}(\nu, J)$ values computed using the B86SRP68-DF2 functional, green for ($\nu = 0$) and magenta for ($\nu = 1$), for H_2 (a) and D_2 (b) + Au(111) as a function of J. The experimental measured were obtained using method A2.

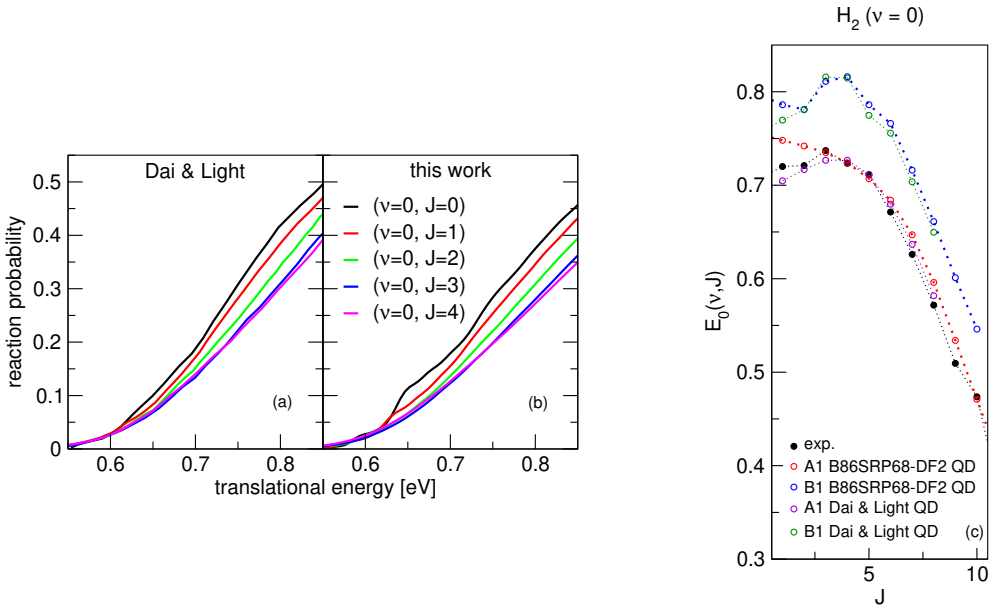

Figure S4: Panel a and b show degeneracy averaged reaction probabilities for ($\nu = 0, J \in [0, 4]$) for H_2 + Cu(111). The results in panel a are the original results of Dai and Light [13], panel b shows our results obtained using the same potential. $E_{1/2}(\nu, J)$ parameters calculated using the QD method are shown in panel c, with experimental results shown in black, [8] and B86SRP68-DF2 results in red and blue. The $E_{1/2}(\nu, J)$ parameters for the LEPS PES used by Dai and Light [13] (purple, green) have been obtained from our QD calculations using the same LEPS PES. [12]

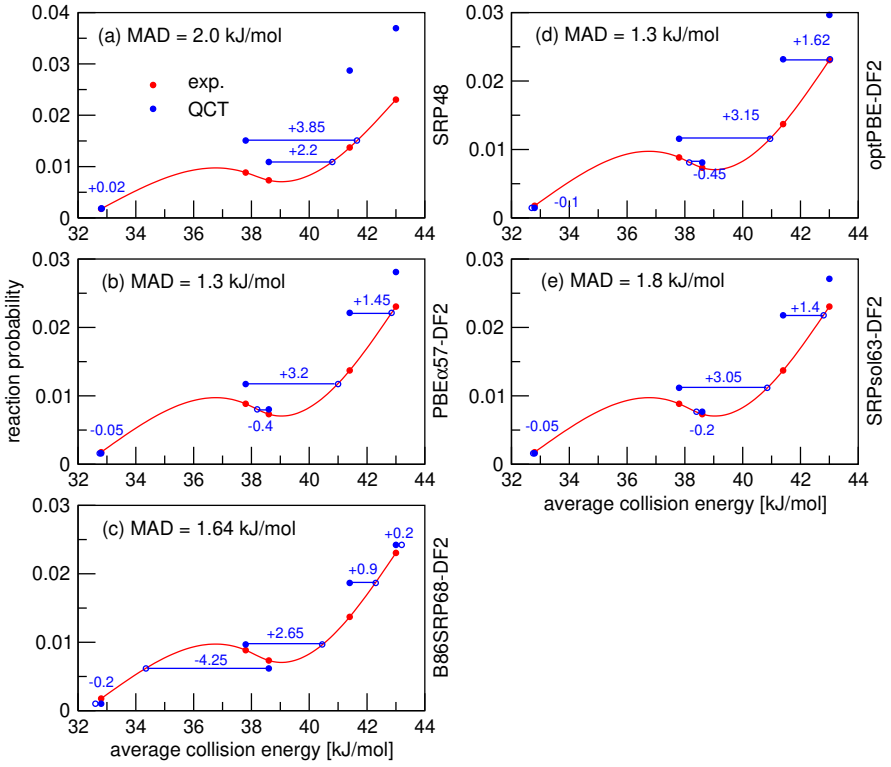

Figure S5: Molecular beam reaction probabilities for D_2 reacting on Cu(111). Experimental values are shown in red.[4] QCT results are shown in blue. The values next to each data point denote the shift along the translational energy axis from the computed reaction probability to the interpolated experimental reaction probability in kJ/mol.

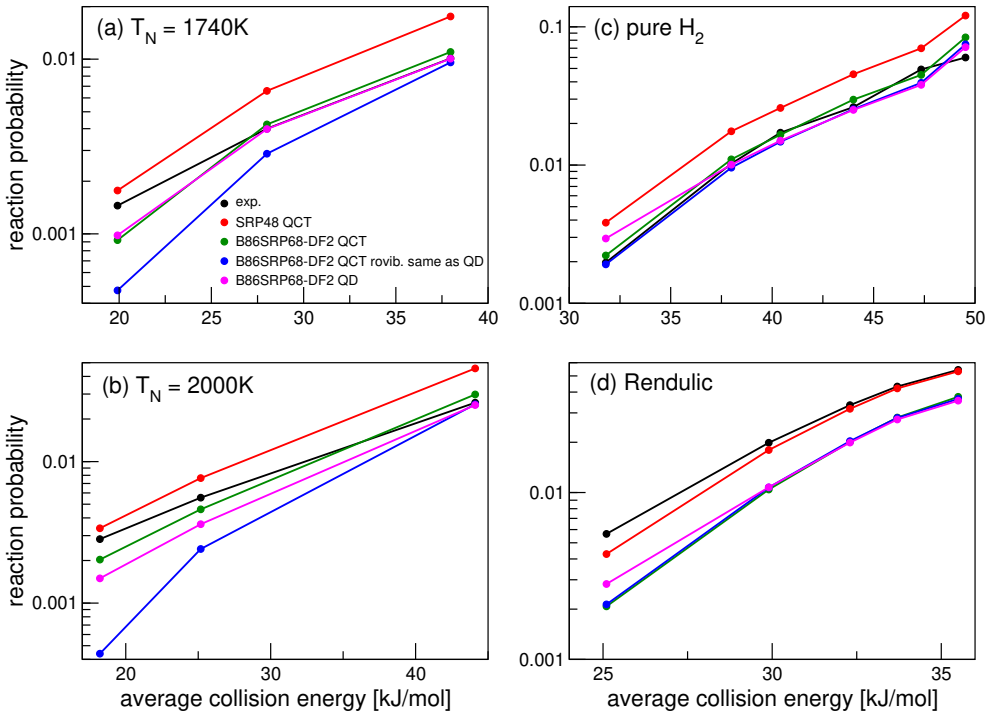

Figure S6: Molecular beam reaction probabilities for H_2 reacting on Cu(111). Experimental values are shown in black,[5] SRP48 QCT results in red, B86SRP68-DF2 QCT results in green, B86SRP68-DF2 QCT results based on the same rovibrational states as taken into account in the QD calculations are shown in blue, and B86SRP68-DF2 QD results in magenta.

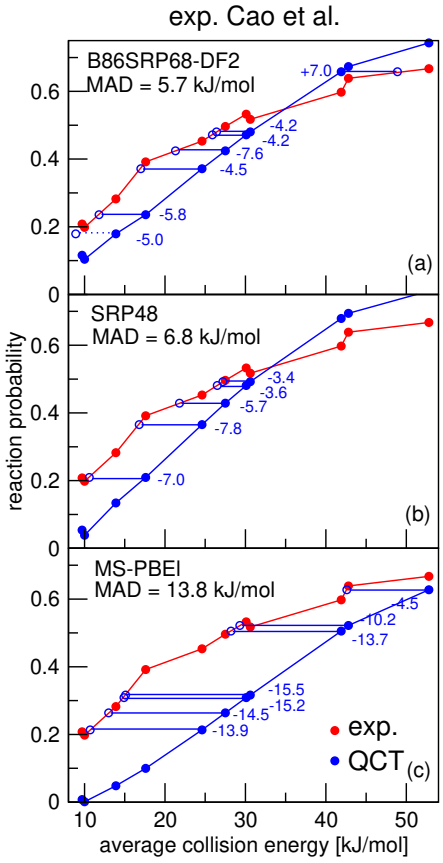

Figure S7: Molecular beam reaction probabilities for D_2 reacting on Pt(111) for the B86SRP68-DF2, SRP48 and MS-PBEl functionals. Experimental values are shown in red.[17] QCT results are shown in blue. The values next to each data point denote the shift along the translational energy axis from the computed reaction probability to the interpolated experimental reaction probability.

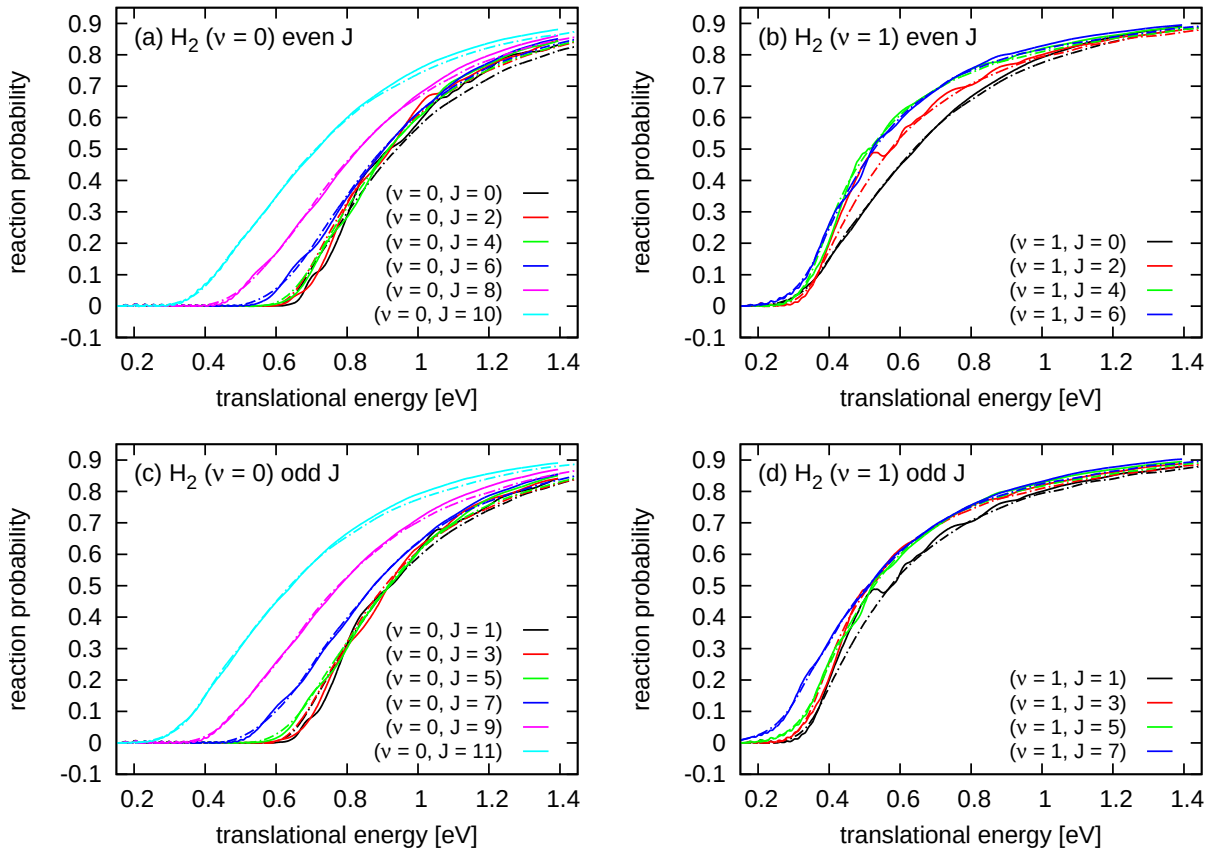

Figure S8: Degeneracy averaged reaction probabilities for H_2 reacting on Cu(111), obtained using the B86SRP68-DF2 functional. Solid lined correspond to QD results, dot-dashed lines correspond to QCT results.

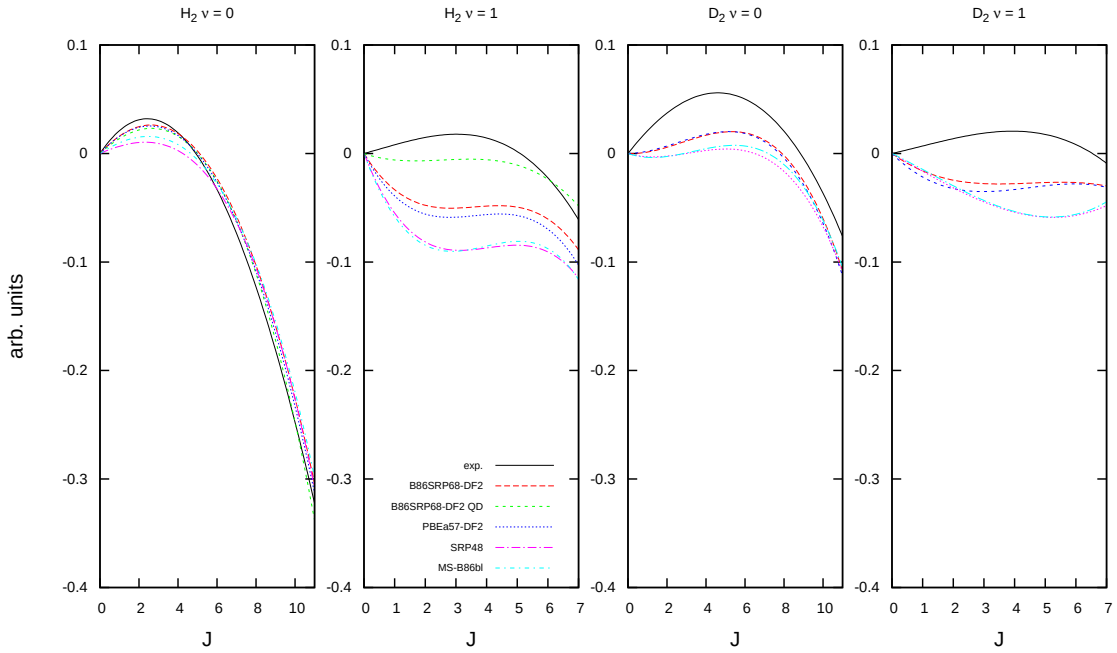

Figure S9: The trend in the J-dependence of the $E_{1/2}(\nu, J)$ parameters calculated using procedure B1 as a function of J for the H_2 (D_2) + Cu(111) system. Here the trend is represented by third degree polynomial fits of the calculated and experimental[8] results, plotted here without the y-axis offset for easy comparison.

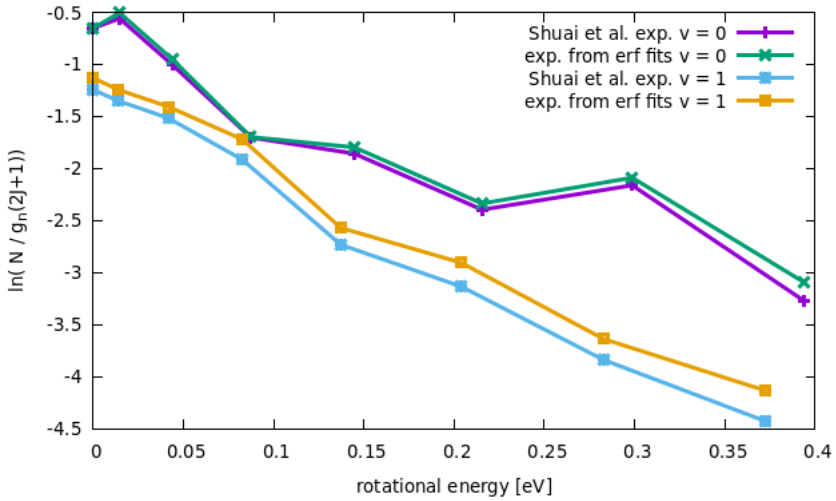

Figure S10: Rovibrational state populations of H_2 desorbing from Au(111) are plotted against the data for H_2 shown in figure 2 of ref.[11] Here the calculated normalized experimental results based on the error function fits have been obtained by performing the integration in Eq. 18 until 5 eV to be consistent with the procedure used in ref.[11] Additionally, the calculated curves have been shifted such that the calculated value for $(\nu = 0, J = 0)$ matches with the $(\nu = 0, J = 0)$ result reported in ref.,[11] and the calculated results for $(\nu = 1)$ have been shifted by the same amount (+3.0).

Supporting tables

Table S1: Input parameters for the 6D quantum simulations on the reactive scattering of H_2 on Cu(111). All wave packets were propagated until the remaining norm was less then one percent.

	H_2 + Cu(111)						
		0.15 eV - 0.55 eV			0.5 eV - 1.4 eV		
	$(\nu = 1, J = 0, m_J = 0)$	$\nu = 0$ $J \in [0, 7]$	$\nu = 0$ $J \in [8, 11]$	$\nu = 1$ $J \in [0, 7]$	$\nu = 0$ $J \in [0, 7]$	$\nu = 0$ $J \in [8, 11]$	$\nu = 1$ $J \in [0, 7]$
Z_{start} (Bohr)	-1.0	-1.0	-1.0	-1.0	-1.0	-1.0	-1.0
$N_{Z_{spec}}$	280	252	252	252	224	224	224
N_Z	240	198	198	198	192	192	192
ΔZ (Bohr)	0.1	0.1	0.1	0.1	0.1	0.1	0.1
R_{start} (Bohr)	0.8	0.8	0.8	0.8	0.8	0.8	0.8
N_R	64	56	56	56	48	48	48
ΔR (Bohr)	0.15	0.15	0.15	0.15	0.15	0.15	0.15
N_X	20	20	20	20	20	20	20
N_Y	20	20	20	20	20	20	20
N_J	36	26 / 25	32 / 31	36 / 35	36 / 35	42 / 41	40 / 39
N_{m_J}	28	26 / 25	32 / 31	28 / 27	28 / 27	40 / 39	32 / 31
Complex absorbing potentials							
Z^{CAP} start [a_0]	15.2	15.2	15.2	15.2	15.2	15.2	15.2
Z^{CAP} end [a_0]	22.90	18.7	18.7	18.7	18.1	18.1	18.1
Z^{CAP} Optimum [eV]	0.03	0.1	0.1	0.1	0.3	0.3	0.3
Z^{CAP}_{spec} start [a_0]	19.8	19.8	19.8	19.8	18.8	18.8	18.8
Z^{CAP}_{spec} end [a_0]	26.90	24.1	24.1	24.1	21.3	21.3	21.3
Z^{CAP}_{spec} Optimum [eV]	0.05	0.08	0.08	0.08	0.25	0.25	0.25
R^{CAP} start [a_0]	4.55	4.55	4.55	4.55	4.55	4.55	4.55
R^{CAP} end [a_0]	10.25	9.05	9.05	9.05	7.85	7.85	7.85
R^{CAP} optimum [eV]	0.1	0.1	0.1	0.1	0.25	0.25	0.25
Propagation							
Δt [$\hbar/E_h$]	2	2	2	2	2	2	2
t_f [$\hbar/E_h$]	45000	20000	20000	20000	13000	13000	13000
Initial wave packet							
E_{min} [eV]	0.055	0.15	0.15	0.15	0.5	0.5	0.5
E_{max} [eV]	0.45	0.55	0.55	0.55	1.4	1.4	1.4
Z_0 [a_0]	17.50	17.40	17.40	17.40	16.8	16.8	16.8

Table S2: Rovibrational states taken into account, according to their Boltzmann weight, in molecular beam simulations for the QCT and QD methods for all H_2 (D_2) + metal systems.

	$(\nu = 0)J_{\max}$	$(\nu = 1)J_{\max}$	$(\nu = 2)J_{\max}$	$(\nu = 3)J_{\max}$	$(\nu = 4)J_{\max}$
QCT	30	30	30	30	30
QD	11	7	-	-	-

Table S3: Molecular beam parameters taken from experiments performed on the H_2 (D_2) + Cu(111) system and the D_2 + Pt(111) system. The parameters v_0, α, T_n represent the stream velocity of the beam, the width of the beam and the nozzle temperature at an average translational incidence energy $\langle E_i \rangle$. Parameters were taken from (the supporting information of) refs [4,9,18–23]

T_n [K]	$\langle E_i \rangle$ [kJ/mol]	v_0 [m/s]	E_0 [eV]	α [m/s]
Seeded molecular H_2 beams, Auerbach and coworkers [4]				
1740	19.9	3923	0.160	1105
1740	28.1	4892	0.250	1105
1740	38.0	5906	0.364	945
2000	18.2	3857	0.155	995
2000	25.1	4625	0.223	1032
2000	44.1	6431	0.432	886
Seeded molecular D_2 beams, Auerbach and coworkers [4]				
2100	35.4	3925	0.322	816
2100	46.4	4595	0.441	782
2100	62.6	5377	0.829	649
2100	69.2	5658	0.860	717
2100	80.1	6132	0.849	830
Pure molecular H_2 beams, Auerbach and coworkers [4]				
1435	31.7	5417	0.307	826
1465	32.0	5446	0.310	830
1740	38.0	5906	0.364	945
1855	40.5	6139	0.394	899
2000	44.1	6431	0.432	886
2100	47.4	6674	0.465	913
2300	49.7	6590	0.454	1351
Pure molecular D_2 beams, Auerbach and coworkers [4]				
1435	32.8	4014	0.336	299
1790	37.8	4196	0.368	614
1670	38.6	4337	0.393	371
1905	41.4	4374	0.399	685
1975	43.0	4461	0.415	687
Pure molecular H_2 beams, Rendulic and coworkers [21]				
1118.07	25.1	3500	0.12794	1996
1331.89	29.9	3555	0.13200	2342
1438.82	32.3	3380	0.11932	2611
1501.19	35.7	3151	0.10371	2819
1581.35	35.5	3219	0.10816	2903
Seeded molecular D_2 beams, Juurlink and coworkers [22]				
473	10.0	2004.6	0.083	528.7
673	9.7	2127.9	0.095	297.9
673	13.9	2256.8	0.106	741.8
973	17.6	2484.9	0.129	881.7
673	24.6	3204.7	0.214	766.3
873	27.5	3302.7	0.228	906.7
873	30.1	3449.1	0.248	955.3
873	30.6	3521.1	0.259	909.4
1223	41.9	4015.0	0.337	1181.0
1223	42.8	4096.5	0.350	1151.1
1503	52.8	4039.3	0.340	1744.7
Seeded molecular D_2 beams, Groot and coworkers [23]				
300	7.5	1932.3	0.078	193.6
500	12.0	2372.5	0.117	295.1
900	21.1	3090.8	0.199	527.4
1300	30.5	3625.4	0.274	765.6
1700	35.0	3818.9	0.304	908.9
1700	43.9	4051.2	0.342	1261.8
1700	45.0	4268.9	0.380	1097.1

Table S4: Zero-point energy corrected experimental lattice constants[34] in Å and percentage deviations of computed values from the experimental value. The UAPE and the SAPE are the unsigned and signed average percentage differences with the experimental value, respectively.

	Cu		Ag		Au		Ni		Pd		Pt			
	Å	%	Å	%	Å	%	Å	%	Å	%	Å	%	UAPE	SAPE
exp.	3.596		4.062		4.062		3.508		3.876		3.913			
SRP48[10]	3.679	2.30	4.207[24]	3.56	4.202[25]	3.44	3.531	0.65	3.985	2.81	3.998	2.17	2.48	2.48
vdW-DF1[26]	3.697	2.80	4.240	4.38	4.245	4.50	3.570	1.76	4.008	3.40	4.032	3.04	3.31	3.31
vdW-DF2[27]	3.742	4.06	4.308	6.05	4.336	6.74	3.607	2.82	4.077	5.18	4.108	4.98	4.97	4.97
BB86SRP68-DF2	3.639	1.19	4.150	2.16	4.166	2.56	3.528[28]	0.57	3.944	1.75	3.979	1.68	1.65	1.65
SRPsol63-DF2	3.644	1.33	4.157	2.33	4.171	2.68	3.525	0.48	3.949	1.88	3.983	1.78	1.75	1.75
PBEα57-DF2[29]	3.656	1.66	4.176	2.80	4.198	3.34	3.534[28]	0.74	3.970	2.42	4.016[29]	2.63	2.27	2.27
optPBE-DF1[30]	3.649[31]	1.47	4.179	2.88	4.197	3.32			3.972	2.47	4.001	2.24	2.47	2.47
MS-B86bl[32]	3.583	-0.37	4.087	0.61	4.087	0.61	3.478	-0.86	3.895	0.49	3.908	-0.13	0.51	0.06
PBE[33]	3.632[34]	1.00	4.152[34]	2.21	4.154[34]	2.26	3.518[34]	0.28	3.948[34]	1.85	3.985[34]	1.84	1.57	1.57
PBEsol[35]	3.570[34]	-0.73	4.058[34]	-0.10	4.081[34]	0.46	3.463[34]	-1.29	3.882[34]	0.15	3.932[34]	0.48	0.54	-0.17

Table S5: Barrier heights for H_2 reacting on Ag(111). For the bridge site $\phi = 90°$ and $\theta = 90°$, while for the t2b and fcc sites $\phi = 0°$ and $\theta = 90°$. The high symmetry locations are shown in figure 1b, the t2b geometry refers to the COM of the molecule being placed on a top site, with the molecular bond pointing to a bridge site. Barrier heights are in eV, and the barrier positions in Å.

	bridge			t2b			fcc		
	E_b	r_b	Z_b	E_b	r_b	Z_b	E_b	r_b	Z_b
SRP48[24]	1.38	1.27	1.10	1.69	1.57	1.51	1.70	1.67	1.34
B86SRP68-DF2	1.379	1.286	1.125	1.614	1.549	1.510	1.608	1.591	1.354
PBEα57-DF2	1.409	1.292	1.114	1.640	1.555	1.511	1.613	1.586	1.348
MS-PBEl	1.288	1.230	1.116	1.534	1.508	1.493	1.601	1.566	1.314

Table S6: Barrier heights for H_2 reacting on Au(111). For the bridge site $\phi = 90°$ and $\theta = 90°$, for the t2b site $\phi = 0°$ and $\theta = 90°$, and for the t2h site $\phi = 0°$ and $\theta = 30°$. The high symmetry locations are shown in figure 1b, the t2b geometry refers to the COM of the molecule being placed on a top site, with the molecular bond pointing to a bridge site. Barrier heights are in eV, and the barrier positions in Å. Additionally the energetic corrugation, ξ, is shown in eV as well.

	bridge			t2b			t2h $\phi = 30°$			ξ
	E_b	r_b	Z_b	E_b	r_b	Z_b	E_b	r_b	Z_b	
PBE	1.245	1.187	1.096	1.237	1.504	1.468	1.637	1.685	1.549	0.392
SRP48[25]	1.407	1.180	1.089	1.382	1.493	1.470	1.783	1.689	1.552	0.376
PBEα57-DF2	1.496	1.232	1.071	1.340	1.492	1.469	1.707	1.664	1.558	0.211
B86SRP68-DF2	1.470	1.218	1.091	1.333	1.480	1.470	1.704	1.659	1.556	0.234
MS-PBEl[32]	1.432	1.144	1.127	1.301	1.433	1.466	1.701	1.578	1.538	0.269
MS-B86bl[32]	1.481	1.142	1.130	1.355	1.438	1.467	1.753	1.583	1.539	0.272

Table S7: Barrier heights for H_2 reacting on Pt(111). For the bridge site $\phi = 90°$ and $\theta = 90°$, for the t2b site $\phi = 0°$ and $\theta = 90°$, and for the t2h site $\phi = 0°$ and $\theta = 30°$. The high symmetry locations are shown in figure 1b, the t2b geometry refers to the COM of the molecule being placed on a top site, with the molecular bond pointing to a bridge site. Barrier heights are in eV, and the barrier positions in Å.

	t2b early			t2b late			bridge			t2h $\phi = 30°$		
	E_b	r_b	Z_b	E_b	r_b	Z_b	E_b	r_b	Z_b	E_b	r_b	Z_b
SRP48	0.096	0.769	2.256				0.473	0.831	1.628	0.252	0.802	1.860
B86SRP68-DF2	0.050	0.776	2.157				0.505	0.853	1.547	0.246	0.816	1.778
PBEα57-DF2[29]	-0.008	0.769	2.202	-0.055	1.096	1.549	0.275	0.837	1.777	0.200	0.837	1.679
MS-PBEl[32]	0.145	0.766	2.205	-0.035	1.096	1.529	0.616	0.838	1.599	0.339	0.800	1.840

Table S8: Van der Waals well depths and positions for Cu(111), Ag(111), Au(111) and Pt(111).

Cu(111)	Z [Å]	E_{vdW} [meV]
exp.	3.51,[36] 2.71[37]	29.5,[36] 22.2[37]
SRP48[9]	4.38	3.73
vdW-DF1	3.77	52.4
vdW-DF2	3.58	39.0
B86SRP68-DF2	3.74	34.3
PBEα57-DF2	3.34	56.7
SRPsol63-DF2	3.71	41.8
optPBE-DF2[31]	3.52	46.9
Ag(111)		
exp.[38]	1.98	32.5
SRP48[24]	4.42	2.3
B86SRP68-DF2	3.75	33.3
PBEα57-DF2	3.39	56.1
Au(111)		
exp.[37]	2.2	40.0
SRP48[25]	4.26	3.0
B86SRP68-DF2	3.62	41.4
PBEα57-DF2	3.30	68.7
Pt(111)		
exp.		55,[39] 76[40]
SRP48	4.14	5.5
B86SRP68-DF2	3.48	48.0
PBEα57-DF2	3.24	72.4

Table S9: Mean absolute and mean signed deviations (MADs and MSDs, in kJ/mol) for the simulated molecular beam experiments presented in section 3.2, in comparison to the respective experiments.

H_2 / D_2 + Cu(111)	D_2 T_N = 2100K		pure D_2		pure H_2		H_2 Rendulic[21]		H_2 T_N = 2000K		H_2 T_N = 1740K	
exp.[4]	MAD	MSD	MAD	MSD	MAD	MSD	MAD	MSD	MAD	MSD	MAD	MSD
SRP48	3.7	3.7	2.0	2.0	2.8	2.8	0.3	-0.3	1.6	1.6	2.6	2.6
B86SRP68-DF2	1.3	-0.5	1.6	-0.1	0.5	0.3	2.5	-2.5	1.9	-1.9	0.4	0.4
SRPsol63-DF2	2.2	0.9	1.2	1.1	0.8	0.8	2.0	-2.0	0.2	0.2	0.9	0.5
PBEα57-DF2[29]	2.3	0.6	1.3	1.1	1.2	1.2	2.1	-2.1	0.8	0.8	1.7	1.7
optPBE-DF2	2.6	1.4	1.3	1.1	1.6	1.6	1.9	-1.9	0.6	0.6	1.4	1.4
MS-B86bl[32]	1.7	0.5	1.2	-0.8	0.3	0.2	2.0	-2.0	2.8	-2.8	0.6	0.6

D_2 + Pt(111)	exp. Luntz[41]		exp. Cao[17]	
	MAD	MSD	MAD	MSD
PBEα57-DF2	1.1	0.19	1.9	-1.1
SRP48	3.5	-3.1	6.8	-6.8
B86SRP68-DF2	3.1	-3.1	5.7	-3.5
MS-PBE[32]	13.4	-13.4	13.8	-13.8

D_2 + Ag(111)	exp. Hodgson[42]	
	MAD	MSD
SRP48[24]	8.4	-8.4
B86SRP68-DF2	4.6	-4.6
PBEα57-DF2[29]	4.3	-4.3
MS-PBEl[32]	4.5	-4.5

Table S10: Mean absolute and mean signed deviations of the theoretical $E_{1/2}(\nu, J)$ parameters from the experimental $E_0(\nu, J)$ values for Cu(111)[8] and Au(111).[11]

Cu(111) Method A1	MAD (eV) H_2			MSD (eV) H_2			MAD (eV) D_2			MSD (eV) D_2		
	total	$\nu=0$	$\nu=1$	total	$\nu=0$	$\nu=1$	total	$\nu=0$	$\nu=1$	total	$\nu=0$	$\nu=1$
SRP48[9]	0.0434	0.0522	0.0301	0.0373	0.0522	0.0151	0.0254	0.0243	0.0272	-0.0066	-0.0008	-0.0152
MS-B86bl[32]	0.0274	0.0165	0.0438	-0.0149	0.0044	-0.0438	0.0551	0.0440	0.0717	-0.0551	-0.0440	-0.0717
B86SRP68-DF2	0.0209	0.0142	0.0308	-0.0176	-0.0089	-0.0308	0.0663	0.0640	0.0698	-0.0663	-0.0640	-0.0698
B86SRP68-DF2 QD	0.0231	0.0183	0.0303	-0.0222	-0.0169	-0.0303						
Dai and Light[13] QD		0.0091			0.0017							
PBEα57-DF2	0.0140	0.0117	0.0174	0.0040	0.0054	0.0018	0.0573	0.0615	0.0509	-0.0573	-0.0616	-0.0509
SRPsol63-DF2	0.0153	0.0136	0.0177	-0.0025	0.0064	-0.0158	0.0510	0.0487	0.0545	-0.0511	-0.0487	-0.0545
optPBE-DF1[31]	0.0146	0.0147	0.0143	0.0054	0.0111	-0.0032	0.0480	0.0481	0.0478	-0.0480	-0.0615	-0.0478

Cu(111) Method B1	MAD (eV) H_2			MSD (eV) H_2			MAD (eV) D_2			MSD (eV) D_2		
	total	$\nu=0$	$\nu=1$	total	$\nu=0$	$\nu=1$	total	$\nu=0$	$\nu=1$	total	$\nu=0$	$\nu=1$
SRP48[9]	0.0409	0.0317	0.0549	-0.0409	-0.0317	-0.0549	0.0336	0.0252	0.0336	-0.0332	-0.0246	-0.0460
MS-B86bl[32]	0.0826	0.0664	0.1067	-0.0826	-0.0664	-0.1068	0.0712	0.0567	0.0929	-0.0712	-0.0567	-0.0929
B86SRP68-DF2	0.0843	0.0756	0.0974	-0.0843	-0.0756	-0.0974	0.0785	0.0709	0.0898	-0.0785	-0.0709	-0.0897
B86SRP68-DF2 QD	0.0846	0.0812	0.0897	-0.0845	-0.0813	-0.0897						
Dai and Light[13] QD		0.0703			-0.0703							
PBEα57-DF2	0.0676	0.0647	0.0718	-0.0676	-0.0648	-0.0718	0.0674	0.0642	0.0723	-0.0674	-0.0642	-0.0723
SRPsol63-DF2	0.0738	0.0660	0.0855	-0.0738	-0.0660	-0.0855	0.0682	0.0613	0.0785	-0.0682	-0.0613	-0.0785
optPBE-DF1[31]	0.0688	0.0635	0.0768	-0.0688	-0.0635	-0.0767	0.0642	0.0583	0.0729	-0.0642	-0.0583	-0.0729

Au(111) Method B1	MAD (eV) H_2			MSD (eV) H_2			MAD (eV) D_2			MSD (eV) D_2		
	total	$\nu=0$	$\nu=1$	total	$\nu=0$	$\nu=1$	total	$\nu=0$	$\nu=1$	total	$\nu=0$	$\nu=1$
PBE	0.1025	0.1333	0.0718	0.1025	0.1333	0.0718	0.0955	0.1178	0.0734	0.0955	0.1176	0.0733
SRP48[25]	0.0309	0.0468	0.0151	0.0158	0.0468	-0.0151	0.0229	0.0325	0.0133	0.0094	0.0321	-0.0131
PBEα57-DF2	0.0189	0.0241	0.0136	0.0026	0.0177	-0.0125	0.0187	0.0246	0.0127	0.0125	0.0246	0.0005
B86SRP68-DF2	0.0270	0.0457	0.0083	0.0217	0.0457	-0.0022	0.0190	0.0275	0.0105	0.0113	0.0275	-0.0050
optPBE-DF1[25]	0.0260	0.0225	0.0259	-0.0044	0.0206	-0.0296	0.0212	0.0116	0.0309	-0.0143	0.0023	-0.0307
MS-PBEl[32]	0.0329	0.0393	0.0264	0.0028	0.0320	-0.0264	0.0270	0.0116	0.0105	0.0212	0.0435	-0.0009

Au(111) Method B2	MAD (eV) H_2			MSD (eV) H_2			MAD (eV) D_2			MSD (eV) D_2		
	total	$\nu=0$	$\nu=1$	total	$\nu=0$	$\nu=1$	total	$\nu=0$	$\nu=1$	total	$\nu=0$	$\nu=1$
PBE	0.0464	0.0471	0.0457	-0.0463	-0.0470	-0.0457	0.0579	0.0551	0.0607	-0.0579	-0.0551	-0.0607
SRP48[25]	0.0891	0.0774	0.1008	-0.0891	-0.0774	-0.1008	0.0948	0.0856	0.1041	-0.0948	-0.0856	-0.1041
PBEα57-DF2	0.1050	0.1143	0.0958	-0.1050	-0.1143	-0.0958	0.0957	0.0905	0.1009	-0.0957	-0.0905	-0.1009
B86SRP68-DF2	0.0854	0.0797	0.0911	-0.0854	-0.0797	-0.0911	0.0955	0.0888	0.1015	-0.0951	-0.0888	-0.1015
optPBE-DF1[25]	0.0959	0.0860	0.1058	-0.0959	-0.0860	-0.1058	0.1037	0.0952	0.1123	-0.1037	-0.0952	-0.1123
MS-PBEl[32]	0.1057	0.1043	0.1072	-0.1057	-0.1043	-0.1072	0.0918	0.0836	0.1000	-0.0835	-0.0551	-0.1120

References

(1) Feit, M.; Fleck Jr, J.; Steiger, A. Solution of the Schrödinger equation by a spectral method. *J. Comput. Phys.* **1982**, *47*, 412–433.

(2) Vibok, A.; Balint-Kurti, G. Parametrization of complex absorbing potentials for time-dependent quantum dynamics. *J. Phys. Chem.* **1992**, *96*, 8712–8719.

(3) Balint-Kurti, G. G.; Dixon, R. N.; Marston, C. C. Grid methods for solving the Schrödinger equation and time dependent quantum dynamics of molecular photofragmentation and reactive scattering processes. *Int. Rev. Phys. Chem.* **1992**, *11*, 317–344.

(4) Michelsen, H.; Rettner, C.; Auerbach, D.; Zare, R. Effect of rotation on the translational and vibrational energy dependence of the dissociative adsorption of D_2 on Cu(111). *J. Chem. Phys.* **1993**, *98*, 8294–8307.

(5) Rettner, C.; Michelsen, H.; Auerbach, D. Quantum-state-specific dynamics of the dissociative adsorption and associative desorption of H_2 at a Cu(111) surface. *J. Chem. Phys.* **1995**, *102*, 4625–4641.

(6) Michelsen, H.; Rettner, C.; Auerbach, D. On the influence of surface temperature on adsorption and desorption in the D_2/Cu(111) system. *Surf. Sci.* **1992**, *272*, 65–72.

(7) Rettner, C.; Auerbach, D.; Michelsen, H. Dynamical studies of the interaction of D_2 with a Cu(111) surface. *J. Vac. Sci. Technol. A* **1992**, *10*, 2282–2286.

(8) Kaufmann, S.; Shuai, Q.; Auerbach, D. J.; Schwarzer, D.; Wodtke, A. M. Associative desorption of hydrogen isotopologues from copper surfaces: characterization of two reaction mechanisms. *J. Chem. Phys.* **2018**, *148*, 194703.

(9) Díaz, C.; Pijper, E.; Olsen, R.; Busnengo, H.; Auerbach, D.; Kroes, G. Chemically accurate simulation of a prototypical surface reaction: H_2 dissociation on Cu(111). *Science* **2009**, *326*, 832–834.

(10) Nattino, F.; Genova, A.; Guijt, M.; Muzas, A. S.; Díaz, C.; Auerbach, D. J.; Kroes, G.-J. Dissociation and recombination of D_2 on Cu(111): Ab initio molecular dynamics calculations and improved analysis of desorption experiments. *J. Chem. Phys.* **2014**, *141*, 124705.

(11) Shuai, Q.; Kaufmann, S.; Auerbach, D. J.; Schwarzer, D.; Wodtke, A. M. Evidence for electron–hole pair excitation in the associative desorption of H_2 and D_2 from Au(111). *J. Phys. Chem. Lett.* **2017**, *8*, 1657–1663.

(12) Dai, J.; Zhang, J. Z. Quantum adsorption dynamics of a diatomic molecule on surface: Four-dimensional fixed-site model for H2 on Cu (111). *The Journal of chemical physics* **1995**, *102*, 6280–6289.

(13) Dai, J.; Light, J. C. The steric effect in a full dimensional quantum dynamics simulation for the dissociative adsorption of H_2 on Cu(111). *J. Chem. Phys.* **1998**, *108*, 7816–7820.

(14) Somers, M.; Kingma, S.; Pijper, E.; Kroes, G.; Lemoine, D. Six-dimensional quantum dynamics of scattering of (ν = 0, j= 0) H_2 and D_2 from Cu(111): test of two LEPS potential energy surfaces. *Chem. Phys. Lett.* **2002**, *360*, 390–399.

(15) Hammer, B.; Scheffler, M.; Jacobsen, K. W.; Nørskov, J. K. Multidimensional potential energy surface for H_2 dissociation over Cu(111). *Phys. Rev. Lett.* **1994**, *73*, 1400.

(16) Busnengo, H.; Salin, A.; Dong, W. Representation of the 6D potential energy surface for a diatomic molecule near a solid surface. *J. Chem. Phys.* **2000**, *112*, 7641–7651.

(17) Cao, K.; Füchsel, G.; Kleyn, A. W.; Juurlink, L. B. Hydrogen adsorption and desorption from Cu(111) and Cu(211). *Phys. Chem. Chem. Phys.* **2018**, *20*, 22477–22488.

(18) Díaz, C.; Olsen, R. A.; Auerbach, D. J.; Kroes, G.-J. Six-dimensional dynamics study of reactive and non reactive scattering of H_2 from Cu(111) using a chemically accurate potential energy surface. *Phys. Chem. Chem. Phys.* **2010**, *12*, 6499–519.

(19) Ghassemi, E. N.; Somers, M. F.; Kroes, G.-J. Assessment of two problems of specific reaction parameter density functional theory: sticking and diffraction of H_2 on Pt(111). *J. Phys. Chem. C* **2019**, *123*, 10406–10418.

(20) Wijzenbroek, M.; Kroes, G. The effect of the exchange-correlation functional on H_2 dissociation on Ru(0001). *J. Chem. Phys.* **2014**, *140*, 084702.

(21) Berger, H.; Leisch, M.; Winkler, A.; Rendulic, K. A search for vibrational contributions to the activated adsorption of H_2 on copper. *Chem. Phys. Lett.* **1990**, *175*, 425–428.

(22) Cao, K.; van Lent, R.; Kleyn, A.; Juurlink, L. A molecular beam study of D_2 dissociation on Pt(111): testing SRP-DFT calculations. *Chem. Phys. Lett.* **2018**, *706*, 680–683.

(23) Groot, I.; Ueta, H.; Van der Niet, M.; Kleyn, A.; Juurlink, L. Supersonic molecular beam studies of dissociative adsorption of H_2 on Ru(0001). *J. Chem. Phys.* **2007**, *127*, 244701.

(24) Nour Ghassemi, E.; Somers, M.; Kroes, G.-J. Test of the transferability of the specific reaction parameter functional for H_2+ Cu(111) to D_2 + Ag(111). *J. Phys. Chem. C* **2018**, *122*, 22939–22952.

(25) Wijzenbroek, M.; Helstone, D.; Meyer, J.; Kroes, G.-J. Dynamics of H_2 dissociation on the close-packed (111) surface of the noblest metal: H_2 + Au(111). *J. Chem. Phys.* **2016**, *145*, 144701.

(26) Dion, M.; Rydberg, H.; Schröder, E.; Langreth, D. C.; Lundqvist, B. I. Van der Waals density functional for general geometries. *Phys. rev. lett.* **2004**, *92*, 246401.

(27) Lee, K.; Murray, É. D.; Kong, L.; Lundqvist, B. I.; Langreth, D. C. Higher-accuracy van der Waals density functional. *Phys. Rev. B* **2010**, *82*, 081101.

(28) Tchakoua, T.; Smeets, E. W. F.; Somers, M. F.; Kroes, G.-J. Towards a specific reaction

parameter density functional for H_2 + Ni(111): comparison of theory with molecular beam sticking experiments. *J. Phys. Chem. C* **2019**,

(29) Ghassemi, E. N.; Wijzenbroek, M.; Somers, M. F.; Kroes, G.-J. Chemically accurate simulation of dissociative chemisorption of D_2 on Pt(111). *Chem. Phys. Lett.* **2017**, *683*, 329–335.

(30) Klimeš, J.; Bowler, D. R.; Michaelides, A. Chemical accuracy for the van der Waals density functional. *J. Phys. Condens. Matter* **2009**, *22*, 022201.

(31) Wijzenbroek, M.; Klein, D. M.; Smits, B.; Somers, M. F.; Kroes, G.-J. Performance of a non-local van der Waals density functional on the dissociation of H_2 on metal surfaces. *J. Phys. Chem. A* **2015**, *119*, 12146–12158.

(32) Smeets, E. W. F.; Voss, J.; Kroes, G.-J. Specific reaction parameter density functional based on the meta-generalized gradient approximation: application to H_2 + Cu(111) and H_2 + Ag(111). *J. Phys. Chem. A* **2019**,

(33) Perdew, J. P.; Burke, K.; Ernzerhof, M. Generalized gradient approximation made simple. *Phys. Rev. Lett.* **1996**, *77*, 3865.

(34) Haas, P.; Tran, F.; Blaha, P. Calculation of the lattice constant of solids with semilocal functionals. *Phys. Rev. B* **2009**, *79*, 085104.

(35) Perdew, J. P.; Ruzsinszky, A.; Csonka, G. I.; Vydrov, O. A.; Scuseria, G. E.; Constantin, L. A.; Zhou, X.; Burke, K. Restoring the density-gradient expansion for exchange in solids and surfaces. *Phys. Rev. Lett.* **2008**, *100*, 136406.

(36) Andersson, S.; Persson, M. Sticking in the physisorption well: influence of surface structure. *Phys. Rev. Lett.* **1993**, *70*, 202.

(37) Harten, U.; Toennies, J. P.; Wöll, C. Molecular beam translational spectroscopy of physisorption bound states of molecules on metal surfaces. I. HD on Cu(111) and Au(111) single crystal surfaces. *J. Chem. Phys.* **1986**, *85*, 2249–2258.

(38) Yu, C.; Whaley, K. B.; Hogg, C. S.; Sibener, S. J. Investigation of the spatially isotropic component of the laterally averaged molecular hydrogen/Ag(111) physisorption potential. *J. Chem. Phys.* **1985**, *83*, 4217–4234.

(39) Cowin, J. P.; Yu, C.-F.; Sibener, S. J.; Wharton, L. HD scattering from Pt(111): rotational excitation probabilities. *J. Chem. Phys.* **1983**, *79*, 3537–3549.

(40) Poelsema, B.; Lenz, K.; Comsa, G. The dissociative adsorption of hydrogen on defect-free Pt(111). *J. Phys. Condens. Matter* **2010**, *22*, 304006.

(41) Luntz, A.; Brown, J.; Williams, M. Molecular beam studies of H_2 and D_2 dissociative chemisorption on Pt(111). *J. Chem. Phys.* **1990**, *93*, 5240–5246.

(42) Hodgson, A.; Samson, P.; Wight, A.; Cottrell, C. Rotational excitation and vibrational relaxation of H_2 (ν= 1, J= 0) Scattered from Cu(111). *Phys. Rev. Lett.* **1997**, *78*, 963.